

**EXPERIMENTAL STUDY OF THE PHOTON STRUCTURE FUNCTION  $F_2$   
IN THE HIGH  $Q^2$  REGION**

JADE Collaboration

W. BARTEL, D. CORDS, G. DIETRICH, P. DITTMANN<sup>1</sup>, R. EICHLER<sup>2</sup>, R. FELST,  
D. HAIDT, H. KREHBIEL, K. MEIER, B. NAROSKA, J. OLSSON, L.H. O'NEILL<sup>3</sup>, P. STEFFEN  
*Deutsche Elektronen-Synchrotron DESY, Hamburg, Germany*

E. ELSER, A. PETERSEN, P. WARMING, G. WEBER  
*II. Institut für Experimentalphysik der Universität Hamburg, Germany*

S. BETHKE, J. HEINTZE, G. HEINZELMANN, K.H. HELLENBRAND, R.D. HEUER,  
J. von KROGH, P. LENNERT, S. KAWABATA<sup>4</sup>, S. KOMAMIYA, H. MATSUMURA,  
T. NOZAKI, H. RIESEBERG, A. WAGNER  
*Physikalisches Institut der Universität Heidelberg, Germany*

A. BELL, F. FOSTER, G. HUGHES, H. WRIEDT  
*University of Lancaster, England*

J. ALLISON, A.H. BALL, G. BAMFORD, R. BARLOW, C. BOWDERY, I.P. DUERDOTH,  
I. GLENDINNING, F.K. LOEBINGER, A.A. MACBETH, H. McCANN, H.E. MILLS,  
P.G. MURPHY, P. ROWE, K. STEPHENS  
*University of Manchester, England*

D. CLARKE, M.C. GODDARD, R. MARSHALL, G.F. PEARCE  
*Rutherford Appleton Laboratory, Chilton, England*

and

J. KANZAKI, T. KOBAYASHI, M. KOSHIBA, M. MINOWA, M. NOZAKI, S. ODAKA,  
S. ORITO, A. SATO, H. TAKEDA, Y. TOTSUKA, Y. WATANABE<sup>4</sup>, S. YAMADA  
and C. YANAGISAWA<sup>5</sup>  
*Lab. of Int. Coll. on Elementary Particle Physics and Department of Physics, University of Tokyo, Japan*

Received 13 October 1982

We report on a measurement of the process  $e^+e^- \rightarrow e^+e^- + \text{hadrons}$ , where one of the scattered electrons is detected at large angles, with an average  $Q^2$  of 23 GeV<sup>2</sup>. The results are analysed in terms of the photon structure function  $F_2$  and are compared with QCD predictions.

<sup>1</sup> Deceased.

<sup>2</sup> Present address: Labor für Hochenergiephysik der ETH-Zürich, Villigen, Switzerland.

<sup>3</sup> Present address: Bell Laboratories, Whippany, NJ, USA.

<sup>4</sup> Present address: KEK, Oho-Machi, Tsukuba-Gun, Ibaraki-Ken, Japan.

<sup>5</sup> Present address: Rutherford Appleton Laboratory, Chilton, England.

Deep inelastic electron-photon scattering,  
 $e + \gamma \rightarrow e + \text{hadrons}$ , (1)

provides a good test of quantum chromodynamics, QCD. The cross section is believed to be dominated by the pointlike contribution at high  $Q^2$  (four-momentum transfer squared), which can be calculated by perturbative QCD [1]. The measurement of the two-photon initiated hadron production,

$e^+e^- \rightarrow e^+e^- + \text{hadrons}$ , (2)

provides an opportunity to study reaction (1) if one of the scattered electrons is detected at a large angle while the other electron is scattered under small angles, which is usually the case if it is not detected (single tag condition) [2,3]. The basic diagram of reaction (2) is shown in fig. 1a.

Under the single tag condition, the cross section of reaction (2) is given, to a good approximation, by the cross section of reaction (1), multiplied by a flux factor of quasi real photons  $N(z, \Theta_{2\max})$  [4],

$$\sigma(ee \rightarrow ee + X) = \int \sigma(e + \gamma \rightarrow e + X) N(z, \Theta_{2\max}) dz. \quad (3)$$

The function  $N(z, \Theta_{2\max})$ , which provides the number of quasi real photons per  $dz$ , is obtained from the

equivalent photon approximation [4,5],

$$N(z, \Theta_{2\max}) = (\alpha/\pi z) \{ [1 + (1-z)^2] \times \ln \{ (E/m_e)[(1-z)/z] \Theta_{2\max} \} - 1 + z \}, \quad (4)$$

with  $z = E_\gamma/E$ ,  $E$  = beam energy,  $E_\gamma$  = energy of quasi real photon,  $\Theta_{2\max}$  = the maximum scattering angle of the undetected electron and  $m_e$  the electron mass.

In terms of the photon structure functions  $F_2$  and  $F_\rho$  the cross section of deep inelastic electron-photon scattering is given by [4]

$$d\sigma/dE' d(\cos \Theta) = [4\pi\alpha^2 E'/(Q^4 y)] \times \{ [1 + (1-y)^2] F_2(x, Q^2) - (2xy^2) F_\rho(y) \}. \quad (5)$$

$Q^2$  and the scaling variables  $x$  and  $y$  are given by:  $Q^2 = 4EE' \sin^2(\Theta/2)$ ,  $x = Q^2/(Q^2 + W^2)$  and  $y = 1 - (E'/E) \cos^2(\Theta/2)$ , where  $E'$  and  $\Theta$  are the energy and the polar angle of the tagged electron, respectively and  $W$  is the total CM energy of the produced hadron system. The second term of eq. (5) is much smaller than the first one, since the average  $y^2$  in this experiment is about 0.07 due to the selection criteria described below. Also QCD predicts the value of  $F_\rho$  to be smaller than that of  $F_2$  in the  $Q^2$  region of the present experiment. The term  $F_\rho$  is therefore neglected in the analysis. A first experimental analysis of this sort at  $\langle Q^2 \rangle = 5 \text{ GeV}^2$  was reported by the PLUTO Collaboration [6].

The data of the present analysis have been taken with the JADE detector at the  $e^+e^-$  colliding beam facility PETRA. The JADE detector has been described elsewhere [7] and here we mention only those features which were essential for this analysis. The tagging of the electrons was carried out using the two arrays of endcap lead-glass counters which cover the angular range from 245 to 500 mrad with respect to the beams. Charged tracks were detected with the central drift chamber (jet chamber) [8] covering 97% of the solid angle and situated in a magnetic field of 4.8 kG. Photons and electrons were detected in the lead-glass shower counters, covering 90% of the solid angle.

The hadronic two-photon events of reaction (2) were selected by applying the following criteria:

(a) The detection of an electron is required in one of the two arrays of endcap lead-glass counters with an energy exceeding  $0.5 E_{\text{beam}}$ . In order to remove

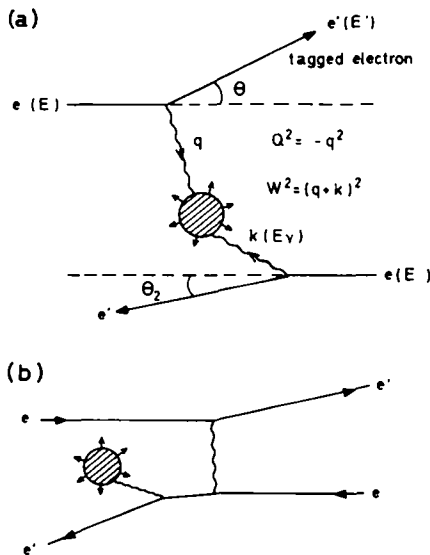


Fig. 1. (a) Feynman diagram of  $e^+e^- \rightarrow e^+e^- + \text{hadrons}$ . (b) Feynman diagram of inelastic Compton scattering.

the effects of the counter edges, the angular range of the tagged electron was restricted to  $\Theta = 265\text{--}428$  mrad. These selection criteria yield  $Q^2$  values ranging from 10 to 60 GeV<sup>2</sup>, on average  $\langle Q^2 \rangle = 23$  GeV<sup>2</sup>. In addition, a track in the central chamber with at least 10 hits had to be associated with the tagged lead-glass cluster. (b) The absence of a second high energy electron with an energy in excess of  $0.25 E_{\text{beam}}$  elsewhere in the whole lead-glass arrays was required. (c) Only events with  $W_{\text{vis}} > 1$  GeV were accepted. Here  $W_{\text{vis}}$  is the visible CM energy of the produced hadron system and is calculated by means of the measured momenta of charged tracks and photons assuming pion masses for all charged tracks. (d) At least three additional charged tracks or two additional charged tracks plus at least one photon were demanded. The charged tracks were required to have transverse momentum  $> 0.1$  GeV/c and  $\cos \vartheta_i < 0.970$  where  $\vartheta_i$  is the polar angle of the track with respect to the beam line. Tracks due to converted photons were not included. Photons were detected as clusters in the barrel- and endcap lead-glass counters and were required to have energies larger than 0.1 GeV and  $\cos \vartheta_\gamma < 0.970$ , with  $\vartheta_\gamma$  the polar angle of the photon. The cuts (b) and (d) suppressed the dominant background originating from the QED processes  $e^+e^- \rightarrow e^+e^-$ ,  $e^+e^- \rightarrow e^+e^-e^+e^-$ ,  $e^+e^- \rightarrow e^+e^-\mu^+\mu^-$  and their higher order contributions like  $e^+e^- \rightarrow e^+e^-\gamma$ , to a level of about 10% of the selected events. QED processes which could not be excluded by these cuts either contained hard photons or produced electromagnetic showers in the materials in front of the central chamber. These events were finally rejected by scanning all the remaining events and using the  $dE/dx$ , lead-glass and muon chamber information. (e)  $1\gamma$  annihilation events containing hard photons radiated from the initial state constitute a background to reaction (2) because the probability for the photon emitted into the tagging angular range to convert into an  $e^+e^-$  pair is on the average 40%. The resulting  $e^+e^-$  pair usually looks like a single short track thus imitating a tagged electron. On the other hand  $1\gamma$  annihilation events have much smaller longitudinal momentum balance (LMB) than  $2\gamma$  hadronic events. LMB is defined as:  $\text{LMB} = (\cos \Theta / |\cos \Theta|) \sum p_i \cos \vartheta_i$  where the sum is over both charged tracks and photons as well as over the tagged electron and  $\Theta$  is the polar angle of the tagged electron. Therefore the

event was rejected if the tagged track had a  $dE/dx$  value larger than one standard deviation away from that expected for a single electron, where  $dE/dx$  was measured in the jet chamber [8], and in addition LMB was smaller than 7.5 GeV/c. Monte Carlo calculations [9,10] show that about 55% of the  $1\gamma$  annihilation events imitating reaction (2) were rejected by these cuts while only about 2% of the events from reaction (2) are lost with these cuts.

176 events survived these cuts for an integrated luminosity of 20.2 pb<sup>-1</sup> at an average beam energy of 16.8 GeV.

These events were corrected for the following remaining background contributions: (1)  $e^+e^- \rightarrow e^+e^-\tau^+\tau^-$ : This background was calculated using Monte Carlo techniques and the number of events was found to be  $25 \pm 2.5$ . (2)  $e^+e^- \rightarrow \tau^+\tau^-$ : 4.6  $\pm$  1.6 background events were obtained using Monte Carlo estimates. (3) Inelastic Compton scattering (fig. 1b): This background was calculated using the cross section formula given in ref. [1] and the resulting number was 4.1  $\pm$  0.3 events. (4) Beam-gas events: From the vertex distribution along the beam line a background of 3.8  $\pm$  1.1 events was estimated. (5) Hadronic  $1\gamma$  annihilation events with initial radiation: The number of remaining annihilation events was estimated to be 14  $\pm$  5.5 from a comparison of the observed LMB distributions at small LMB with model calculations for  $2\gamma$  production [10] and  $1\gamma$  annihilation [9]. After subtraction of these background contributions, 125  $\pm$  15 events remained. The errors quoted above are statistical only.

In order to compare these data with various theoretical predictions, the  $x_{\text{vis}}$  distribution was calculated, with  $x_{\text{vis}} = Q^2 / (Q^2 + W_{\text{vis}}^2)$ .  $W_{\text{vis}}$  is on the average 30% smaller than the true  $W$  due to the loss of particles outside the limited acceptance. Thus  $x_{\text{vis}}$  is normally larger than the true  $x$ .  $Q^2$  is calculated from the measured energy and polar angle of the scattered electron. The  $x_{\text{vis}}$  distributions from the various background sources have been estimated using Monte Carlo techniques except for the beam-gas events where the real data with different vertex cuts were used. These distributions have been subtracted from the data bin by bin. The resulting  $x_{\text{vis}}$  distribution is shown in fig. 2<sup>+1</sup>.

<sup>+1</sup> For footnote see next page.

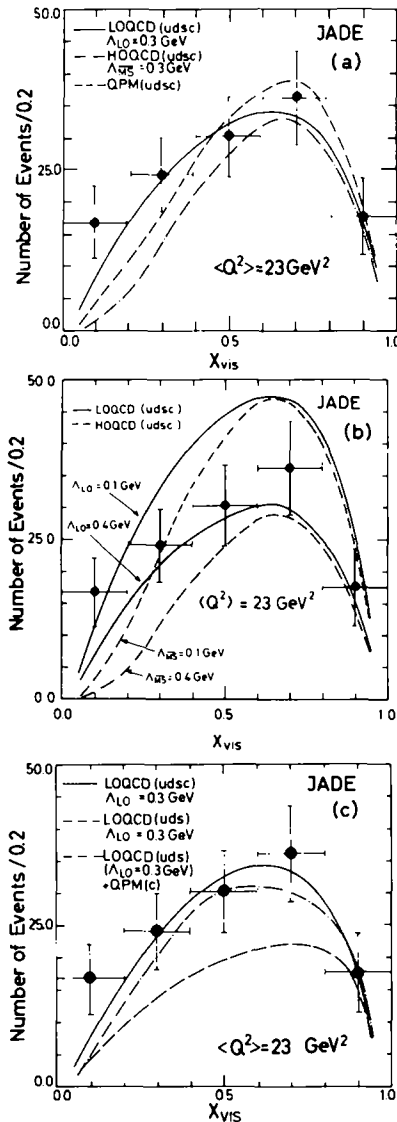


Fig. 2. (a)  $x_{vis}$  distribution. Solid curve = LOQCD (u, d, s, c) with  $\Lambda_{LO} = 0.3$  GeV. Dashed-dotted curve = HOQCD (u, d, s, c) with  $\Lambda_{MS} = 0.3$  GeV. Dashed curve = QPM (u, d, s, c). (b)  $x_{vis}$  distribution. Solid curves = LOQCD (u, d, s, c) with  $\Lambda_{LO} = 0.1$  and  $0.4$  GeV. Dashed curves = HOQCD (u, d, s, c) with  $\Lambda_{MS} = 0.1$  and  $0.4$  GeV. (c)  $x_{vis}$  distribution. Solid curve = LOQCD (u, d, s, c) with  $\Lambda_{LO} = 0.3$  GeV. Dashed-dotted curve = LOQCD (u, d, s) with  $\Lambda_{LO} = 0.3$  GeV plus QPM (c). Dashed curve = LOQCD (u, d, s) with  $\Lambda_{LO} = 0.3$  GeV.

<sup>†1</sup> Preliminary results of this experiment are given in ref. [11]. In the old analysis the  $\tau$  background was not corrected for and also the absence of c quark distributions in the high x region was not properly taken into account in the plot of  $F_2(x, Q^2)$ .

Fig. 2 also contains several theoretical predictions resulting from a computer simulation of reaction (2) in the JADE detector. In this simulation first  $e^+e^- \rightarrow e^+e^-q\bar{q}$  events were produced [10] according to eqs. (3), (4) and (5) using the  $F_2(x, Q^2)$  functions discussed below. The hadronic part of  $F_2$ , which arises from a vector meson like component of the photon, was neglected since the hadronic part of  $F_2$  is expected to be small at high  $Q^2$  and to contribute mainly in the small  $x(x_{vis})$  region [1]. The quark masses were assumed to be:  $m_u = m_d = 300 \text{ MeV}/c^2$ ,  $m_s = 500 \text{ MeV}/c^2$  and  $m_c = 1.6 \text{ GeV}/c^2$ . For this calculation the photon flux given by eq. (4) was slightly modified, since it is not accurate enough for  $\Theta_{2max} = 245 \text{ mrad}$  as given by the acceptance of the endcap lead-glass counters. For this renormalisation an exact calculation of the process  $ee \rightarrow eeq\bar{q}$  [12] was used. In the second step the quarks were fragmented via the standard Field-Feynman fragmentation scheme [13]. We used the same parameters as employed in our previous analysis of high  $p_t$  jets from two-photon interactions [14]. In the third step the resolution of the jet chamber and lead-glass counters was included. The electron showers in the endcap lead-glass counters were simulated by means of a Monte Carlo program for three-dimensional electromagnetic shower development in lead-glass [15]. In the fourth step the Monte Carlo events were passed through the same analysis programs which were used for the analysis of the real data. Nuclear interactions of charged tracks in the materials in front of the chamber were taken into account. This Monte Carlo simulation of reaction (2) reproduced various observed distributions like multiplicity and momentum distributions of charged particles and photons, the  $Q^2$  distribution of tagged electrons and the  $W_{vis}$  distribution of the produced hadron system rather well.

The following structure functions  $F_2(x, Q^2)$  have been used as input for these calculations:

(a) The quark-parton model function (QPM)

$$F_2(x, Q^2)^{(QPM)} = \frac{3\alpha}{\pi} \sum_{i=u,d,s,c} e_i^4 \{x[x^2 + (1-x)^2] \times \ln(W^2/m_q^2) + 8x^2(1-x) - x\}, \quad (6)$$

where  $e_i$  = quark charge,  $m_q$  = quark mass and  $W^2 = Q^2(1/x - 1)$ . Note that because of the high  $W^2$ , contributions from the c quark have to be included. For the c quark we actually used a more lengthy for-

mula without approximation of the light quark masses [16].

(b) Leading order QCD (LOQCD)

$$F_2(x, Q^2)^{(\text{LOQCD})} = \frac{3\alpha}{\pi} \sum_{i=u,d,s,c} e_i^4 f(x)^{(\text{LOQCD})} \times \ln(Q^2/\Lambda_{\text{LO}}^2), \quad (7)$$

which includes QCD corrections in leading order.  $\Lambda_{\text{LO}}$  is the QCD scale parameter in leading order approximation. Several authors have calculated  $f(x)^{(\text{LOQCD})}$  by different methods and obtained similar results [17–20]. The results of ref. [17] were used in the present analysis. Since no QCD calculations exist which include quark mass effects, we had to use the same  $F_2$  for all flavours. Only phase space effects were taken into account by setting  $F_2$  to zero for the c quark in the range  $x > x_{\text{th}}$  [ $x_{\text{th}} = Q^2/(Q^2 + 4m_c^2)$ ].

(c) Higher order QCD (HOQCD)

$$F_2(x, Q^2)^{(\text{HOQCD})} = \frac{3\alpha}{\pi} \sum_{i=u,d,s,c} e_i^4 \{f(x)^{(\text{LOQCD})} \times \ln(Q^2/\Lambda_{\overline{\text{MS}}}^2) + g(x) \ln[\ln(Q^2/\Lambda_{\overline{\text{MS}}}^2)] + h(x)\}, \quad (8)$$

which includes recent QCD calculations in next to leading order [21–23].  $\Lambda_{\overline{\text{MS}}}$  is the QCD scale parameter in the  $\overline{\text{MS}}$  scheme [24]. We numerically determined the functions  $f(x)^{(\text{LOQCD})}$ ,  $g(x)$  and  $h(x)$  from the results given in ref. [23] and computed  $F_2(x, Q^2)^{(\text{HOQCD})}$  using eq. (8). The contribution from the small  $x$  region where  $F_2$  becomes negative was neglected in the Monte Carlo simulation of the  $x_{\text{vis}}$  distribution<sup>†2</sup>. The same treatment of the c quark was done as for (b).

The resulting  $x_{\text{vis}}$  distributions are shown in figs. 2a–2c. Fig. 2a shows the quark–parton model (QPM) prediction together with the leading order (LOQCD) and higher order QCD (HOQCD) predictions both for  $\Lambda = 0.3$  GeV. All three curves provide a reasonable description of data with the exception of the lowest  $x_{\text{vis}}$ -bin, reflecting a reasonable choice of the quark masses in eq. (6) and of the QCD parameter  $\Lambda$  in eqs. (7) and (8). The high data point in the lowest  $x_{\text{vis}}$ -bin might be due to the contribution from the hadronic (vector meson like) component of the photon which

<sup>†2</sup> The negative value of  $F_2$  in the small  $x$  region which is predicted by HOQCD might be compensated by the additional hadronic component of  $F_2$ . See refs. [23,25].

Table 1

Measured values of  $\Lambda_{\text{LO}}$  and  $\Lambda_{\overline{\text{MS}}}$  for three different models.

Model	$\Lambda_{\text{LO}}$ (GeV)	$\Lambda_{\overline{\text{MS}}}$ (GeV)
QCD (udsc)	0.28 <sup>+0.13</sup> <sub>-0.09</sub>	0.22 <sup>+0.10</sup> <sub>-0.07</sub>
QCD (uds) + QPM (c)	0.21 <sup>+0.17</sup> <sub>-0.09</sub>	0.18 <sup>+0.12</sup> <sub>-0.07</sub>
QCD (uds)	0.07 <sup>+0.05</sup> <sub>-0.03</sub>	0.06 <sup>+0.05</sup> <sub>-0.03</sub>

is expected to be largest in the lowest  $x_{\text{vis}}$ -bin. The curves of fig. 2 are quite sensitive to the parameter  $\Lambda$  as indicated in fig. 2b, and in principle allow its determination. These QCD calculations, however, neglect quark mass effects (except for the phase space effect mentioned above), an approximation not justified for the c quark. The uncertainties introduced by the treatment of the c quark can be estimated from fig. 2c, where the leading order QCD predictions are shown with and without the c quark contribution. Also shown is a curve for which the light quark (u, d, s) contribution was calculated by LOQCD but the c quark contribution was calculated by the QPM. The QCD parameter  $\Lambda$  obtained by fitting the data with the theoretical predictions in the region of  $x_{\text{vis}} > 0.4$  are listed in table 1. These values are consistent with values of  $\Lambda_{\text{LO}} \sim \Lambda_{\overline{\text{MS}}} = 0.1$  to 0.35 GeV obtained from deep inelastic lepton–nucleon scattering experiments [26]. The above  $x_{\text{vis}}$  cut was applied to reduce the possible contribution from the hadronic component of the photon.

LOQCD as well as QPM predict the  $\ln Q^2$  dependence of the photon structure function  $F_2$  for fixed  $x$ . Fig. 3 shows the  $Q^2$  dependence of the func-

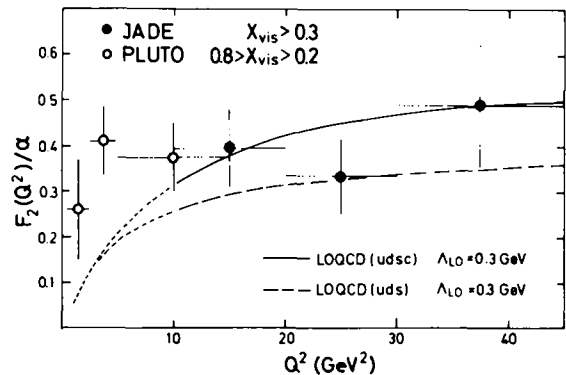


Fig. 3.  $F_2/\alpha$  as a function of  $Q^2$ . Full circles (JADE data) =  $F_2(x, Q^2)/\alpha$  averaged over  $x_{\text{vis}} > 0.3$ . Open circles (PLUTO data) =  $F_2(x, Q^2)/\alpha$  averaged over  $0.2 < x_{\text{vis}} < 0.8$ . Solid curve = LOQCD (u, d, s, c) with  $\Lambda_{\text{LO}} = 0.3$  GeV. Dashed curve = LOQCD (u, d, s) with  $\Lambda_{\text{LO}} = 0.3$  GeV.

tion  $F_2(x, Q^2)$  averaged over the range  $x_{\text{vis}} > 0.3$ , where the correlation between  $Q^2$  and  $x$  is found to be small according to Monte Carlo calculations. Also shown in fig. 3 are the results of a similar analysis at smaller  $Q^2$  by the PLUTO Collaboration [6]. For comparison the LOQCD prediction is shown for  $\Lambda_{\text{LO}} = 0.3$  GeV. The LOQCD prediction without the c quark contribution is separately indicated. It is seen that, while the JADE data are consistent with the LOQCD prediction the lower  $Q^2$  PLUTO points are located above these curves. This might be due to the hadronic contribution to  $F_2$  which is expected to be more significant in the PLUTO data because of the smaller  $Q^2$  [1,6].

In summary, a measurement of the process  $e^+e^- \rightarrow e^+e^- + \text{hadrons}$  was carried out under the single tag condition at an average  $Q^2$  of 23 GeV<sup>2</sup>. The results were analysed in terms of the photon structure function  $F_2$  and they were found to be well described by leading order QCD in the whole  $x_{\text{vis}}$  region. Also quark-parton model as well as higher order QCD predictions agree well with the data except in the small  $x_{\text{vis}}$  region. The QCD parameter  $\Lambda$  was determined to  $\Lambda_{\overline{\text{MS}}} = 0.18 (+0.12, -0.07)$  GeV if higher order corrections are taken into account and if the c quark contribution is taken from the quark-parton model. Future improvements demand not only higher statistics but also a proper treatment of heavy quarks in the perturbative QCD calculations.

We are indebted to the PETRA machine group for their excellent support and to all the engineers and technicians who have participated in the construction and maintenance of the apparatus. This experiment was supported by the UK Science Research Council through the Rutherford Laboratory, by the Educational Ministry of Japan and by the Bundesministerium für Forschung und Technologie. The visiting groups wish to thank the DESY directorate for their hospitality.

### References

- [1] C. Petersen, T.F. Walsh and P.M. Zerwas, Nucl. Phys. B174 (1980) 424.
- [2] S.J. Brodsky, T. Kinoshita and H. Terazawa, Phys. Rev. D4 (1971) 1532.
- [3] T.F. Walsh, Phys. Lett. 36B (1971) 121.
- [4] V.M. Budnev et al., Phys. Rep. 15C (1975) 182.
- [5] C. Carimalo, P. Kessler and J. Parisi, Phys. Rev. D21 (1980) 669.
- [6] PLUTO Collab., Ch. Berger et al., Phys. Lett. 107B (1981) 168.
- [7] JADE Collab., W. Bartel et al., Phys. Lett. 88B (1979) 171; 92B (1980) 206; 99B (1981) 277.
- [8] H. Drumm et al., Nucl. Instrum. Methods 176 (1980) 333; J. Heintze, Nucl. Instrum. Methods 196 (1982) 293; A. Wagner, Proc. Intern. Conf. on Instrumentation for colliding beam physics (SLAC, 1982) SLAC-Report 250, p. 76.
- [9] B. Andersson, G. Gustafson and T. Sjöstrand, Phys. Lett. 94B (1980) 211; T. Sjöstrand, LUTP 80-3 (April, 1980), Errata to LUTP 80-3.
- [10] S. Kawabata, Program Write-Up (1982), unpublished.
- [11] JADE Collab., W. Bartel et al., reported XVIIth Rencontre De Moriond (Les Arcs-Savoie-France, March 1982).
- [12] P. Bhattacharya, J. Smith and G. Grammer, Phys. Rev. D15 (1977) 3267; J. Smith, J.A.M. Vermaseren and G. Grammer, Phys. Rev. D15 (1977) 3280; J.A.M. Vermaseren, Program Write-Up (1978), unpublished.
- [13] R.D. Field and R.P. Feynman, Nucl. Phys. B136 (1978) 1.
- [14] JADE Collab., W. Bartel et al., Phys. Lett. 107B (1981) 163.
- [15] A. Sato, Master Thesis, University of Tokyo (1978), unpublished; K. Messel and J.F. Crawford, Electron-photon shower distribution function tables (Pergamon, London, 1970).
- [16] C.T. Hill and G.G. Ross, Nucl. Phys. B148 (1979) 373.
- [17] E. Witten, Nucl. Phys. B120 (1977) 189.
- [18] C.H. Llewellyn Smith, Phys. Lett. 79B (1978) 83.
- [19] W.R. Frazer and J. Gunion, Phys. Rev. D20 (1979) 147.
- [20] R.J. Dewitt et al., Phys. Rev. D19 (1979) 2046.
- [21] W.A. Bardeen and A.J. Buras, Phys. Rev. D20 (1979) 166.
- [22] D.W. Duke and J.F. Owens, Phys. Rev. D22 (1980) 2280.
- [23] T. Uematsu and T.F. Walsh, Fermilab-PUB-81/55-THY.
- [24] W.A. Bardeen et al., Phys. Rev. D18 (1978) 3998.
- [25] W.A. Bardeen, Proc. 1981 Intern. Symp. on Lepton and photon interactions at high energies (Bonn, 1981) p. 432.
- [26] J. Wotschack, Proc. 1981 Intern. Symp. on Lepton and photon interactions at high energies (Bonn, 1981) p. 461; J. Drees, Proc. 1981 Intern. Symp. on Lepton and photon interactions at high energies (Bonn, 1981) p. 474; F. Eisele, Proc. Xth Intern. Winter Meeting on Fundamental physics and XIIIth GIFT Intern. Seminar on Theoretical physics (Masella, Spain, January 1982).